POLITECNICO
MILANO 1863

SCUOLA DI INGEGNERIA INDUSTRIALE
E DELL'INFORMAZIONE

EXECUTIVE SUMMARY OF THE THESIS

Graphene oxide reduction and decoration with lead sulphide nanoparticles for gas sensing application

TESI MAGISTRALE IN MATERIALS ENGINEERING AND NANOTECHNOLOGY - INGEGNERIA DEI MATERIALI E DELLE NANOTECNOLOGIE

Author: VALENTINA BERLIN

Advisor: ANDREA LI BASSI

Co-advisors: BENOIT HACKENS, SOPHIE HERMANS, FERNANDO MASSA FERNANDES

Academic year: 2021-2022

1. Introduction

The growing concern about the worsening of air quality conditions in highly polluted environments has increased the demand for highly sensitive, inexpensive, and energy-efficient gas sensors for the detection of harmful gasses such as NO_2, NH_3, CO_2, CO and CH_4. To date, the solutions available on the market present limitation related to large production costs, poor portability, and high operating temperatures. In recent years, hybrid functional graphene-based sensors have been proposed as suitable candidates for environmental monitoring, as graphene-derived material can be employed in conjunction with other nanometric structures for the detection of a wide range of chemicals [1]. Among this kind of chemiresistive devices, reduced graphene oxide (rGO) planes decorated with semiconductor nanoparticles present outstanding performances in terms of responsivity and sensitivity due to the combination of superb interaction of the nanocrystals (NCs) with the analyte and great charge transport in rGO. The interest of the scientific community towards the implementation of reduced graphene oxide in gas sensors is justified not only by its remarkable electronic properties, but also because, unlike its pristine counterpart, it enables high-volume production at a relatively low-cost. More specifically, rGO large-scale synthesis involves the oxidation and exfoliation of bulk graphite to yield graphene oxide which, upon chemical or thermal deoxygenation, exhibits an electrical behaviour similar to that of pristine graphene. Different reduction processes have been proposed in literature but they often present low efficiency towards the removal of oxygen functionalities from GO surface [2].

In this thesis, various graphene oxide's reduction techniques have been investigated, namely low-temperatures thermal annealing assisted by ethanol or benzene healing, simple chemical reduction with ascorbic acid, and a combination of solvothermal annealing and chemical reduction in N-methyl-2-pyrrolidone (NMP). The objectives of this project are collectively aimed at the improvement of the effectiveness of these processes, while exploring the possibility of decorating rGO flakes with lead sulphide nanoparticles (PbS NPs) for application in chemiresistive methane sensors.

2. Experimental methods

Sample preparation procedures, graphene oxide's reduction techniques and lead sulphide's synthesis methods are briefly discussed in this paragraph.

2.1. Sample production

Three graphene oxide's suppliers have been considered in this research: Graphenea, Sigma-Aldrich, and Angstron Materials (US). For synthesis purposes, in this short elaborate they will be named GO(A), GO(B), and GO(C), respectively. High concentration GO aqueous dispersions (0.5 mg/mL and 0.25 mg/mL) were produced for morphological and spectroscopic studies. To break the clustered GO, improve the dispersion of GO sheets, and reduce the dimension of the biggest GO flakes, ultrasonic treatment at 45 kHz and 60 W was performed for varying period of time (from 15 minutes to 4 hours). Given the high hydrophobicity of GO(B), stable dispersions were obtained by adding small amount of aqueous ammonia (~100 µl / 10 mL) or by substituting Milli-Q water with NMP. In light of the results of the morphological studies, presented in the next section, GO(A) dispersions (0,025 mg/mL) were employed for the production of the final devices. Finally, homogeneous PbS NPs water dispersions (5 mg/mL) were produced by ultrasonic treatment for 4 hours at 45 kHz and 100 W.

Both graphene oxide flakes and PbS nanocrystals were deposited by drop casting on Si/SiO_2 wafers and ready-made CMOSEnvi™ dies (patented VOCSens). A schematic representation of the latter is reported in Figure 1.

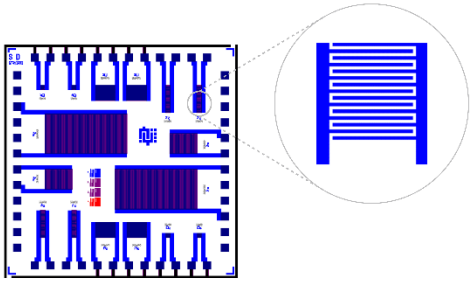

Figure 1: Schematic representation of CMOSEnvi™ dies (patented VOCSens).

2.2. Thermal annealing and healing treatments of graphene oxide samples

The effectiveness of low-temperature thermal annealing processes for the removal of oxygen functional groups from GO surface has been investigated in this work. Ethanol and benzene, instead, have been studied as potential liquid state carbon sources for the restoration of sp^2 domains on GO basal plane. Both processes were conducted in high vacuum conditions and the upper limit to the annealing temperature was chosen to avoid damages to the substrate (CMOSEnvi™ dies). All the samples were subjected to the following heating cycle:

- 30 minutes at 80°C to promote the evaporation of any residual water trace;
- rapid heating up to 320°C to facilitate the removal of oxygen moieties;
- rapid cooling down to room temperature. The lid of the chamber was opened when the thermocouple inside the vacuum chamber registered 30°C.

For both GO(B) and GO(C) samples the high temperature step was maintained for 3 hours, after which a resistance plateau was reached. GO(A) samples were instead treated for longer times (8 hours) in an effort to get measurable resistance values.

2.3. Chemical reduction and solvothermal annealing of graphene oxide samples

Liquid-phase chemical reduction was performed with L-ascorbic acid (L-AA), an environmentally friendly reducing agent that provides highly efficient removal of the oxygen-groups [3]. Both NMP and Milli Q water were tested as reduction medium at different temperatures. For comparison purposes, a simple solvothermal annealing in NMP and a healing treatment with ethanol were carried out by heating the liquid medium up to 199°C. Ascorbic acid and absolute ethanol concentrations were set at 0.8 M. Further details are reported in Table 1.

Table 1: Details about the reduction experiments.

Reduction medium	T_R (°C)
Milli-Q water/Ascorbic acid (0.141 g/mL)	80°C
NMP/Ascorbic acid (0.141 g/mL)	80°C
NMP/Ascorbic acid (0.141 g/mL)	199°C
NMP	199°C
NMP/absolute ethanol (0.369 g/mL)	199°C

2.4. Preparation of PbS nanoparticles

Lead sulphide nanocrystals were synthetized following an easy room temperature process [4]. Lead (II) nitrate ($Pb(NO_3)_2$), sodium sulphate (Na_2S) and 2-mercaptoethanol ($HOCH_2CH_2SH$) (14.3 M) were employed as lead source, sodium source, and capping agent, respectively. First, 1.53 g of $Pb(NO_3)_2$ was dissolved in 50 mL of degassed Milli-Q water (0.1 M concentration) and introduced into a triple-neck round-bottom flask kept under argon flow, to prevent products

oxidation. Then, 100 mL of 0.1 M 2-mercaptoethanol solution was introduced dropwise in the reaction flask via a separatory funnel under stirring. Finally, a solution of 360 mg of sodium sulphate dissolved in 50 mL of Milli-Q water (0.1 M concentration) was introduced in the flask dropwise in the course of 4 hours. The mixture was stirred for ~ 10 hours to ensure the completion of the reaction, reported in Equation 1:

$$Pb(NO_3)_{2\,(aq)} + Na_2S_{(aq)} \rightarrow PbS_{(s)} + 2NaNO_{3\,(aq)} \quad (1)$$

The removal of byproducts and residual organic capping was achieved by repeating three times the centrifugation of the mixture (6000 rmp, 15 minutes) followed by washing with fresh Milli-Q water. The solution was then centrifuged one last time to remove the PbS from aqueous media. The wet paste was later dried at 50°C for 10 hours and crushed with mortar and pestle until obtaining a fine powder.

2.5. Characterization techniques

Graphene oxide flakes and lead sulphide nanoparticles were analysed using several characterization techniques. Scanning electron microscopy (SEM) was employed to evaluate the morphology, the size and the thickness of graphene oxide flakes, to assess the diameter of PbS NPs and verify the decoration of the GO films with the latter. Raman spectroscopy was used to investigate the structural properties and the defectivity of the graphene oxide before and after each treatment. In particular, in the region between 1000 cm^{-1} and 2000 cm^{-1}, where the most significant features of graphene oxide's Raman spectrum are located, Raman curves were fitted with five Lorentzians. The degree of graphitization was then estimated by evaluating the ratio between the relative intensity the D and G peak (I_D/I_G), centered around 1350 cm^{-1} and 1580 cm^{-1}. An example of the five-peak deconvolution of GO Raman spectrum is represented in Figure 2. Carbon/oxygen and sp^2/sp^3 ratios were further studied through X-ray photoelectron spectroscopy (XPS). However, the poor distribution of GO flakes on the substrate complicated the process of identification of the XPS data referring to the actual material of interest. As results, many unreliable data point were eliminated, substantially reducing the data poll to get a relevant statistical analysis of the effect of the reduction processes on GO.

The degree of reduction of the graphene oxide flakes was further evaluated through IV curves acquisition at a low signal probe station.

X-ray fluorescence spectroscopy (XRF) and X-ray diffraction spectroscopy (XRD) were utilized to assess the composition and verify the crystallinity of lead sulphide powders. The data acquired from the fitting of the XRD patterns with pseudo-Voight curves were then employed for the calculation of the average crystallite size through Debye-Scherrer equation, reported in Equation 2:

$$D_{hkl} = \frac{K\lambda}{B_{hkl}\cos\vartheta} \quad (2)$$

where D_{hkl} is the crystallite size, hkl are the Miller indices of the planes being analysed, λ is the X-ray wavelength, B_{hkl} is the width (full-width at half-maximum) of the X-ray diffraction peak in radians, θ is the Bragg angle in radians and K is crystallite-shape factor, equal to 0.9 for cubic structures. Finally, preliminary measurements on the response of rGO/PbS-based devices to methane atmosphere (2%) have been performed in a gas sensing set-up. Temperature (25°C), pressure (1 atm) and relative humidity (43%) were maintained constant during the gas sensing experiments.

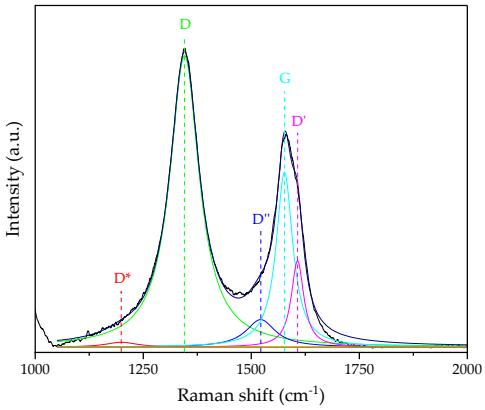

Figure 2: Deconvolution of GO Raman spectrum.

3. Results and discussion

In this paragraph, an overview of the key finding of the analysis conducted on graphene oxide, reduced graphene oxide and lead sulphide nanoparticles will be presented.

3.1. Morphological characterization

The efficiency of the ultrasonication treatment in tuning the size and shape of the graphene oxide flakes was evaluated by observing SEM micrographs of sonicated GO dispersions.

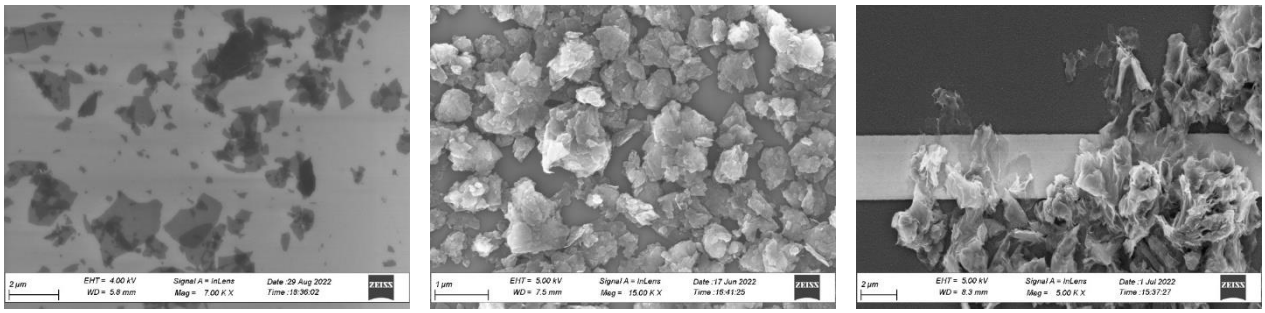

(a) (b) (c)

Figure 3: SEM micrographs of (a) GO(A), (b) GO(B), and (c) GO(C) after ultrasonication treatment.

In particular, it was noticed that the immersion in the ultrasonic bath have a limited effect on the morphology of GO(B), composed of graphite oxide clusters rather than multilayer graphene oxide (Figure 3 (b)), and GO(C), which instead shows an accordion-like structure (Figure 3 (c)). The impossibility to control their morphological characteristics made GO(B) and GO(C) inadequate for the production of the final devices but still useful for studies regarding the efficiency of the healing and thermal reduction procedures.

On the contrary, GO(A) presents wrinkled multilayers graphene flakes, the size and shape of which are easily controlled just by fixing the power and frequency of the ultrasonic bath and adjusting the sonication time (Figure 3 (a)). Therefore, the morphological requirement for the gas sensing devices explored in this work (i.e., flakes flatness and lateral size ~ 1-2 μm) were met by subjecting GO(A) to ultrasonic treatment for 60 minutes at 45 kHz and 100 W.

3.2. Thermal annealing and healing treatments

To investigate the efficiency of thermal annealing procedure alone, the value of the I_D/I_G ratio for the three graphene oxide samples before and after the thermal annealing procedure were first considered. From the analysis of the data reported in Table 2, it can be inferred that during the annealing process oxygen moieties are partially removed with the simultaneous recovery of the graphitic plane structure. This hypothesis is corroborated by the sharp decrease in resistance observed during the heating of the samples. The plots of the resistance and temperature variation during the thermal annealing experiment are reported in Figure 4. The initial strongly insulating behaviour of the samples can be attributed to the small size of the sp^2 domain, which grows as the temperature is increased from 80°C to ~ 325-330°C, resulting in an enhanced electrical conductivity. Recent studies [5] have demonstrated that significant crystallographic changes occur on GO sheets at a temperature between 200°C and 250°C, to which is associated a systematic drop in resistance. However, the limited two-wire resistance measurements range (100 Ω - 100 MΩ) of the digital multimeter employed at the vacuum chamber station did not allow to acquire the resistance data for GO(A) samples. This implies that it was not possible to significantly recover the conductivity of the GO(A) samples through thermal annealing, making the process unsuitable for the reduction of highly oxidized species.

Table 2: ID/IG ratio before and after the thermal annealing

Sample	I_D/I_G ratio Reference	I_D/I_G ratio Annealed
Graphenea's GO	1.79 ± 0.06	1.49 ± 0.03
Sigma-Aldrich's GO	0.98 ± 0.10	0.91 ± 0.08
Angstron Materials' GO	2.13 ± 0.11	1.98 ± 0.18

On the other hand, it was not possible to establish a definitive trend regarding the improvement of the degree of graphitization in presence of a carbon source from the Raman spectra acquired on the thermally annealed and healed samples. XPS data, with all the limitation underlined in the previous paragraph, seems to indicate an increase in the oxygen content after the healing treatment with ethanol, but the limited number of reliable data does not allow to confirm that the ethanol healing treatment was successful. The results concerning the healing treatment with benzene as C-source are instead completely unreliable. Therefore, the analysis on the efficiency of the healing treatment is generally inconclusive. However, the promising results reported in literature about the ability of ethanol to repair GO defect sites in conditions similar to those employed in this work, support the hypothesis that the employment of other

characterization techniques such as FTIR measurements and XRD measurements could prove the effectiveness of ethanol in healing GO flakes.

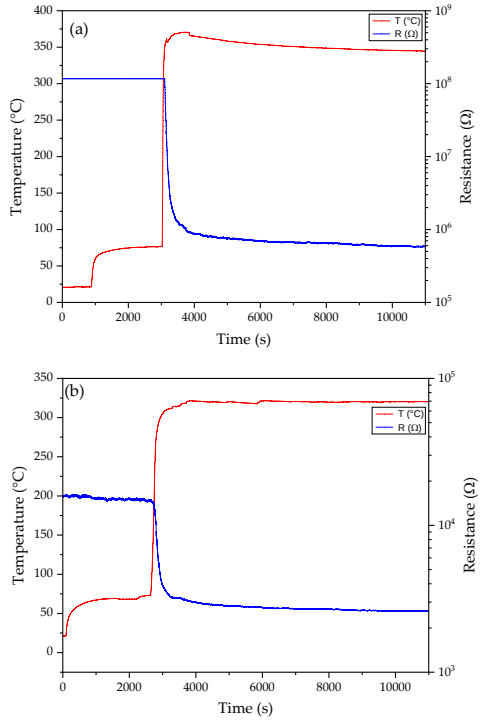

Figure 4: Resistance and temperature variation during the thermal annealing experiments of (a) GO(B) and (b) GO(C).

3.3. Solvothermal annealing and chemical reduction

The data obtained from the Raman spectra analysis of the chemically reduced and thermally annealed samples are reported in Table 3.

Table 3: I_D/I_G ratio after chemical reduction and solvothermal annealing.

Reduction medium	T_R (°C)	I_D/I_G ratio
-	-	1 ± 0.10
Milli-Q water/Ascorbic acid	80°C	0.88 ± 0.04
NMP/Ascorbic acid	80°C	0.87 ± 0.05
NMP	199°C	0.73 ± 0.06
NMP/Ethanol	199°C	0.76 ± 0.08
NMP/ Ascorbic acid	199°C	0.63 ± 0.06

The data follow a well-defined trend: as the temperature of the reducing medium (Milli Q water or NMP) increases, the reduction process becomes more efficient. This tendency can be explained by considering the co-effect of the temperature-accelerated reduction kinetics of ascorbic acid and the oxygen-scavenging character of N-Methyl-2-pyrrolidone at high temperatures. NMP contribution to GO deoxygenation explains also the fact that GO samples subjected to solvothermal treatment alone present a higher degree of reduction compared to the same samples reduced via thermal annealing in vacuum.

Additionally, the resistance values extracted from IV curves measurements, performed before and after each treatment, follows the same trend defined by Raman data. Table 4 reports the initial ($R_{INITIAL}$) and final (R_{FINAL}) resistance values.

Table 4: Resistance values of GO flakes before and after the reduction processes.

Reduction medium	$R_{INITIAL}$ (TΩ)	R_{FINAL} (Ω)
Milli-Q water/ L-AA (80°C)	2.62 ± 1.65	834654.8 ± 21481.9
NMP/L-AA (80°C)	3.68 ± 3.08	16519.1 ± 86.1
NMP (199°C)	4.28 ± 6.08	72301.2 ± 146.8
NMP/Ethanol (199°C)	1.74 ± 2.76	51018.8 ± 100.4
NMP/ L-AA (199°C)	4.92 ±1.28	395.0 ± 0.3
NMP/ L-AA /Ethanol (199°C)	8.34 ± 2.39	232.4 ± 3.55

It is worth noticing that high temperatures seem to promote the interaction of ethanol with the defective site of graphene oxide. This hypothesis, formulated based on the I_D/I_G ratio values, is confirmed by the improvement in resistivity of the samples subjected to ethanol healing, compared to the ones just exposed to high temperatures and ascorbic acid.

A zoomed-in representation of the IV curves (Figure 5) of the reduced samples highlights the progressive improvement of conductivity. For the sample with the highest conductivity, the resistivity decreased by 10 orders of magnitude, a value not yet reported in literature for GO samples reduced via chemical route with ascorbic acid.

From these considerations, it can be stated that chemical reduction with ascorbic acid is a feasible route for the reduction of highly oxidized graphene oxide. The contribution of the solvothermal annealing, possible thanks to the use of a solvent with a high boiling point (NMP, 202°C), is important to allow a sufficient lowering of the resistance of GO. Finally, it has been proven that ethanol healing process at 199°C allows a further increase in conductivity.

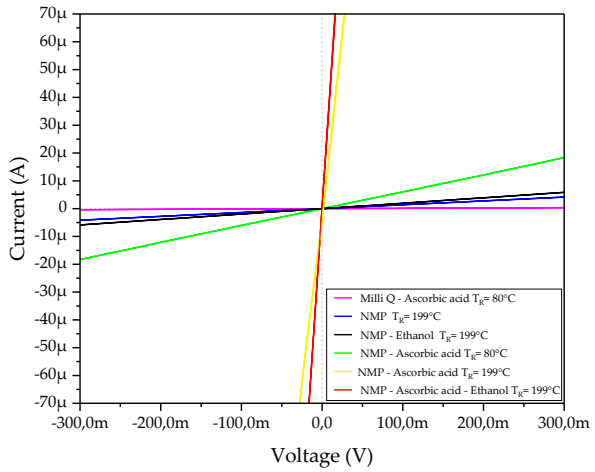

Figure 5: Zoomed I-V characteristics of the devices after the reduction procedure.

3.4. Lead sulphide nanoparticles

Quantitative information about the composition of the PbS powders were gathered through XRF spectroscopy. The two batch of powders, here named PbS_A and PbS_B, used for the production of the final devices presented a lead-to-sulphur ratio compatible with the presence of PbS nanoparticles (Table 5).

Table 5: Pb/S molar ratio

Sample	Pb/S molar ratio
PbS_A	1.272
PbS_B	1.405

XRD patterns of PbS_A and PbS_B are presented in Figure 6 (a) and (b). The two profiles show clearly defined peaks, the broadening of which confirms the crystalline nature of the two powders.

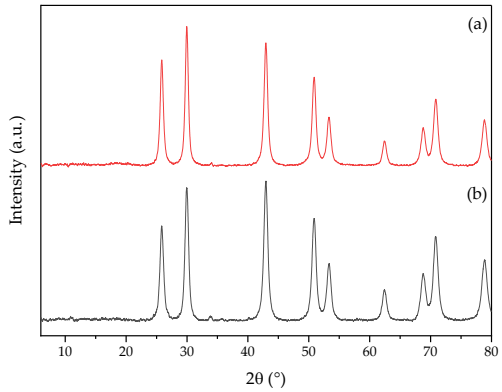

Figure 6: XRD pattern of (a) PbS_A and (b) PbS_B

As mentioned in Section 2.5, the average crystallite size was calculated through the Debye-Scherrer equation. The mean crystallite size (10.801 ± 0.689 and 10.801 ± 0.689, respectively) turned out to be smaller than the exciton Bohr radius of lead sulphite (18 nm), allowing the classification of the PbS crystallites as quantum dots. PbS NPs size and shape was further investigated by SEM imaging, which indicates the presence of spherical particles, with an average diameter of 12.399 ± 2.719 nm for PbS_A and 11.072 ± 3.102 nm for PbS_B, consistent with the size evaluation obtained by the Debye-Scherrer formula. Additionally, the homogeneous PbS NPs' distribution suggests that the sonication time and drop casting techniques have been well optimized.

3.5. Decoration of rGO flakes with lead sulphide nanoparticles

The decoration of the reduced graphene oxide flakes with PbS nanoparticles was achieved by drop casting the latter on the already reduced samples. It can be observed (Figure 7) that PbS nanoparticles tend to strongly adhere to rGO flakes especially in correspondence of the area between metallic fingers. The bath in acetone, methanol and water that follows the drop casting does not seem to affect the distribution of the nanocrystals, that appear homogeneously distributed on top of the graphene oxide flakes.

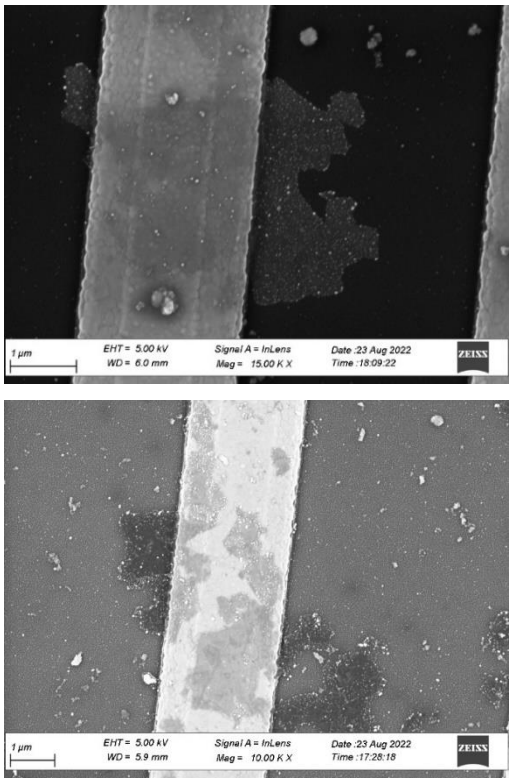

Figure 7: Reduced graphene oxide flakes decorated with lead suphide NPs.

3.6. Preliminary gas sensing measurements

Finally, preliminary measurements of the devices' response to methane atmosphere (2%) have been performed in the gas sensing measurements setup. The results of multiple tests indicate no sensitivity towards the analyte. Knowing that the device's sensitivity mechanism is related to the interaction of methane molecules with the surface of the lead nanoparticles, it can be hypothesized that the cause of the absence of sensitivity is related to the uncontrolled growth of the oxide layer around PbS nanocrystals. Therefore, further investigation about the chemical and thermal stability of the calchogenides quantum-dots are required.

4. Conclusions

In conclusion, it can be stated that the objectives defined at the beginning of the project have been generally accomplished. Different GO's reduction methods have been investigated and new protocols have been developed to improve the effectiveness of GO's deoxygenation process. In particular, the combination of chemical reduction with ascorbic acid and solvothermal annealing in NMP at 199°C proved to be extremely effective in removing oxygen moieties and recovering of the sp^2-hybridized carbon planes. Accordingly, the initial resistance decreased by 10 orders of magnitude, a number greater than anything recorded in the literature so far for GO reduction with ascorbic acid. Moreover, a simple water-based synthesis route for lead sulphide nanoparticles has been explored and the yielded PbS quantum dots were employed in rGO flakes' decoration. The successful adhesion of the small sensing element to the basal conductive plane allowed to perform preliminary measurements of the devices' response to methane atmosphere, which indicate no sensitivity towards the analyte; in this regard, further investigation about the chemical and thermal stability of the calchogenides quantum-dots should be conducted.

At last, it is worth noting that there is still potential for improvement in some areas of this work. For instance, additional studies on the possibility of substituting N-Methyl-2-pyrrolidone with less hazardous and more environmentally friendly high boiling point solvents are required. Additionally, XPS measurements should be collected on pressed graphene oxide and reduced graphene oxide powders, to avoid surface inhomogeneities and substrate interference, that have greatly affected the results of the analysis presented in this work. Finally, additional data about the mechanism of removal of oxygen containing group at different reduction temperatures could be acquired through FTIR analysis; instead, conductive AFM could be employed to obtain more information about the conduction mechanism in reduced rGO flakes.

References

[1] Y. Jian, W. Hu, Z. Zhao, P. Cheng, H. Haick, M. Yao and W. Wu, "Gas sensors based on chemi-resistive hybrid functional nanomaterials," *Nano-Micro Letters,* vol. 12, no. 1, 2020.

[2] D. J. Buckley, N. C. Black, E. G. Castanon, C. Melios, M. Hardman and O. Kazakova, "Frontiers of graphene and 2D material-based gas sensors for environmental monitoring," *IOP Publishing,* vol. 3, no. 7, 2020.

[3] M. Palomba, G. Carotenuto and A. Longo, "A brief review: the use of L-ascorbic acid as a green of graphene oxide," *Materials,* vol. 15, no. 18, 2022.

[4] A. Mosahebfard, H. D. Jahromi and M. H. Sheikhi, "Highly sensitive, room temperature methane gas sensor based on lead sulfide colloidal nanocrystals," *IEEE Sensor Journal,* vol. 16, no. 11, pp. 4174-4179, 2016.

[5] H. Ramamoorthy, K. Buapan, T. Chiawchan, K. Thamkrongart and R. Somphonsane, "Exploration of the temperature-dependent correlations present in the structural, morphological and electrical properties of thermally reduced free-standing graphene oxide paper.," *Journal of Material Science,* vol. 56, p. 15134–15150, 2021.

5. Acknowledgements

I would like to thank Benoit Hackens, Sophie Hermans and Andrea Li Bassi for the opportunity to undertake this thesis work. A special thanks to Fernando Massa Fernandes, my mentor during these months, without whom this project would not have been possible. Finally, the most important thanks to my family and my boyfriend for having supported me financially and emotionally during these years.